Electronic Supplemental Information for

Enhanced Carrier Transport of Monolayer $MoSe_2$ through Interlayer Coupling with In Situ Grown Metal-Organic Frameworks

Shan Wang,[ad] Qing Zhang,[acd] Aiqing Fan,[ad] Lin Li,[bd] and Dechao Geng*[ade]

[a] Key Laboratory of Organic Integrated Circuit, Ministry of Education & Tianjin Key Laboratory of Molecular Optoelectronic Sciences, Department of Chemistry, School of Science, Tianjin University and Collaborative Innovation Center of Chemical Science and Engineering, Tianjin 300072, P. R. China;

[b] College of Chemistry, Tianjin Normal University, Tianjin 300387, China;

[c] School of Advanced Materials, Peking University Shenzhen Graduate School, Peking c University, Shenzhen 518055, China;

[d] Beijing National Laboratory for Molecular Sciences, Beijing 100190, China;

[e] Haihe Laboratory of Sustainable Chemical Transformations, Tianjin 300192, China;

*E-mail address: gengdechao_1987@tju.edu.cn

Experimental Section

Synthesis of $MoSe_2$ monolayers

$MoSe_2$ was prepared by CVD method in a single-temperature tube furnace. Molybdenum trioxide (MoO_3) with 99.95% purity and selenium (Se) with 99.99% purity from Aladdin were used as precursors for $MoSe_2$ growth. The Si/SiO_2 substrate was cleaned using acetone, isopropanol and ethanol before growth. A mixture of 3 mg MoO_3 powder and NaCl powder (3 mg, 99%, Aladdin) was placed on a boat, and then the substrate was inverted on top, after which it was placed in a CVD system. Ar (300 sccm) was first introduced for 15 min to exclude the effect of oxygen and water. When the temperature was raised to 850 °C, 100 mg of selenium powder was pushed to the reaction position (upstream area, 21 cm from the substrate) by a magnet. Afterwards, $MoSe_2$ films were obtained after 15 min of growth in a mixed gas (100 sccm Ar and 5 sccm H_2) atmosphere.

Preparation of heterojunction field-effect transistors

A gold electrode was transferred to $MoSe_2$ by probing. $MoSe_2/SiO_2/Si$ was used as a novel substrate for the in situ growth of MOF thin films on a liquid surface. Firstly, 6.6 mg of Nickel Chloride Hexahydrate ($NiCl_2{\cdot}6H_2O$, Aladdin) and 10.0 mg of 2,3,6,7,10,11-Hexaminohexaphenylmethylhexachlorohydrogen (HITP·6HCl, Aladdin) were weighed in two beakers according to the Sheberla method. Subsequently, 5 mL of deionised water was added to each beaker, and the resulting solution was entirely dissolved by magnetic

stirring. Subsequently, 300 μL of ammonia was added dropwise to the $NiCl_2$ solution, forming a turbid mixture. This mixture was then slowly added dropwise to the HITP·6HCl solution, leading to the gradual development of turbidity in the mixed reaction solution. Once the solution turned grey-black, it was transferred to a water bath kept at 60°C. Then, the $MoSe_2/SiO_2/Si$ substrate was rapidly inverted on the surface of the reaction solution. After 60 min remove them and dry in an oven at 80°C for 5 hours to obtain heterojunction field effect transistors. In order to exclude the effect of water on the material, comparative experiments were executed. The PL spectral and electrical property results showed that water had a weak effect on the material properties.

Material Characterisation

The morphology of $MoSe_2$ crystals and heterojunctions was observed using a Nikon ECLIPSE Ci POL polarising microscope. The more detailed morphological analyses are performed using SEM (Hitachi SU8010). TEM was conducted using the JEM-2800, while the SAED tests were performed on both the JEM-2800 (ROYAL PHILIPS, Amsterdam, Netherlands) and Thermo Scientific Talos F200X. EDS mapping images were collected using the TEM system. XRD measurements were carried out in reflection mode at 45 kV and 200 mA with monochromatic Cu Kα radiation utilising a Rigaku Smartlab diffractometer. The thickness of crystals was confirmed by AFM (Bruker Dimension ICON-PT). XPS spectra were collected from PHI 5000 Versaprobe III XPS (ULVACPHI.INC). Raman and PL spectroscopies were performed on Renishaw InVia using an excitation

wavelength of 532 nm. UPS spectra were collected from Thermo escalab 250Xi. UV–vis absorption spectrum of MOFs was measured with a SHZMADZU UV-3600 Plus spectrophotometer. The current-voltage (I-V) curves were measured using a probe station (Keithley 4200MPW-600). The photoresponse characteristics were evaluated by a laser generator with tunable power density. The laser power density was measured in situ by a light intensity meter PM100D. The TRPL experiments were performed using transient absorption spectrometer LP980.

Considering the non-linear behaviour of the transfer characteristics, the channel current can be expressed as:

$$I_d = \frac{W}{L}\mu C_i V_d |V_g - V_{th}|^{\alpha}$$

where L and W are the channel length and width, respectively, μ is the field-effect mobility, C_i is the insulator capacitance perunit of area, V_{th} is the threshold voltage and $\alpha \geqslant 1$ is a dimensionless parameter that accounts for a possible V_g-dependence of the mobility. According to equation, when the I_d–V_g curve is linear, α = 1, and the carrier mobility μ was determined from the following equation:

$$\mu = \frac{dI_d}{dV_g} \times \frac{L}{WC_i V_d}$$

where L and W are the channel length and width, and C_i is the insulator capacitance per unit of area.

The dopant-induced charge carrier density increase (Δn) was calculated from Equation:

$$\Delta n = C_i \frac{\Delta V_{th}}{e}$$

where ΔV_{th} is the difference in threshold voltage V_{th} between $MoSe_2$ and the heterojunction and e is the elementary charge (1.6×10^{-19} C).

The independent Boson model equation was as follows:

$$\Gamma(T) = \Gamma_0 + \sigma T + \frac{\Gamma_0 p}{e^{\hbar\omega_0 p / k_B T} - 1}$$

where Γ_0 is the inhomogenous broadening contribution, σ is the exciton-acoustic phonointeraction (T > 0, neglected), $\Gamma_0 p$ is the exciton-optical phonon contribution, k_B is the Boltzmann constant (8.617×10^{-5} eV K^{-1}), and $\hbar\omega_0 p$ is the optical phonon energy.

The temperature-dependent intensity was plotted, and the curve could be fitted using the Arrhenius equation:

$$\frac{1}{I(T)} = \frac{1}{I_0}\left(1 + Ae^{-E_B / k_B T}\right)$$

Where $I(T)$ is the temperature-dependent PL intensity, and I_0 is the PL intensity at 0 K, A is the densities of the centres, and E_B is the activation energy. k_B is Boltzmann constant, 8.617×10^{-5} eV/K.

Supporting Figures

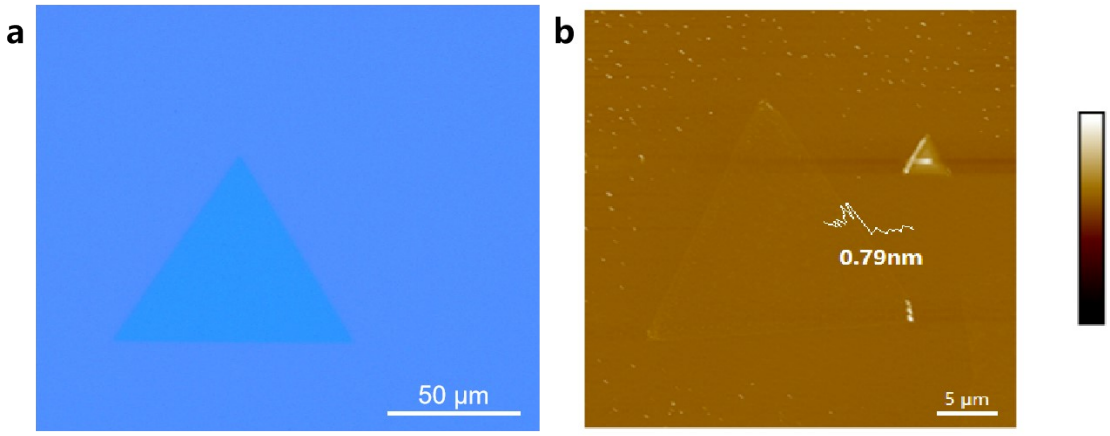

Fig. S1. (a) Optical microscope images and (b) AFM height images of $MoSe_2$ layers.

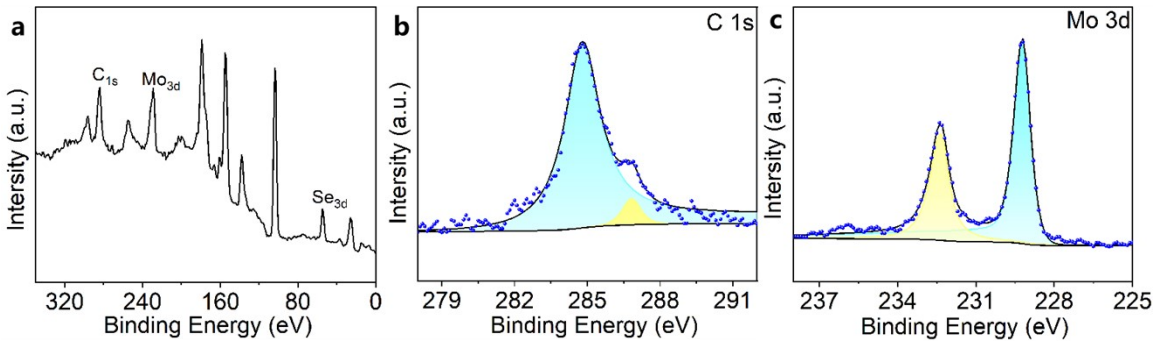

Fig. S2. (a) Full spectrum of XPS conducted on the samples, containing C, Mo and Se elements. (b-c) High-resolution spectrums of C element and Mo element, respectively.

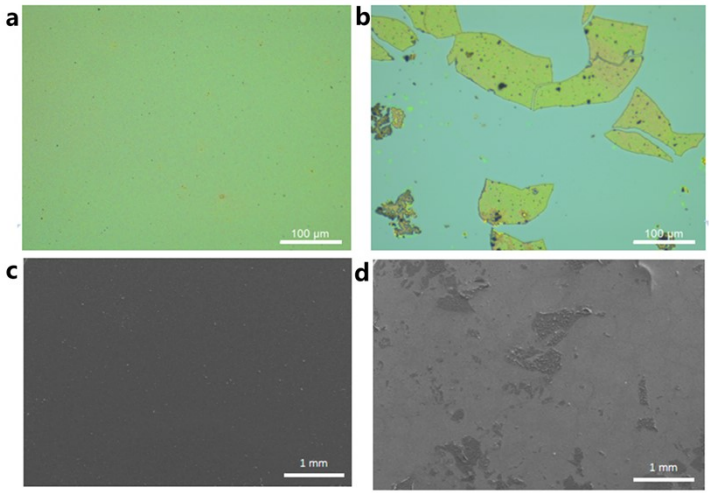

Fig. S3. Optical microscope images and SEM images of Ni-MOF crystals synthesised by different methods. (a, c) *In situ* growth and (b, d) transferred samples.

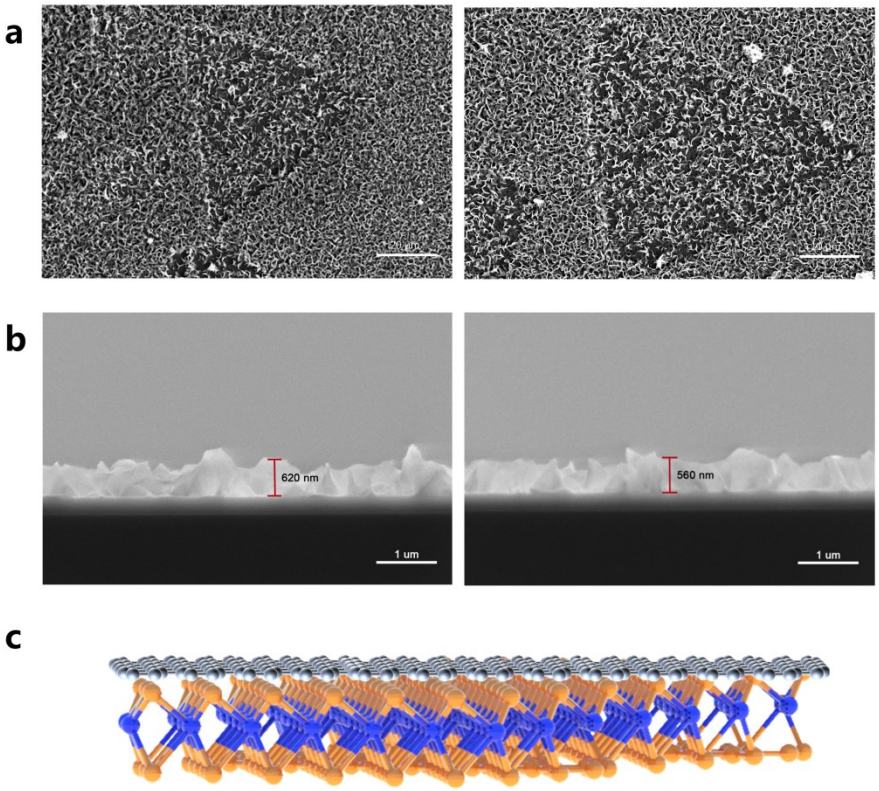

Fig. S4. SEM images of (a) horizontal plane and (b) cross-section of heterojunctions.; (c) Heterojunctions assembled by van der Waals forces.

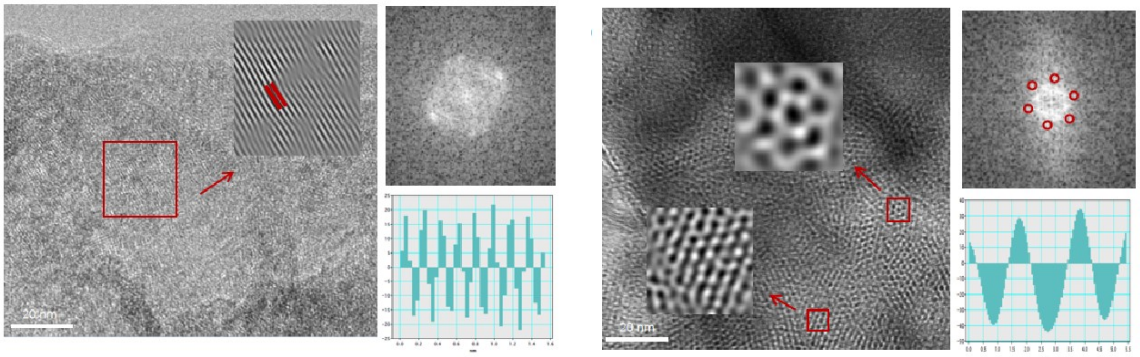

Fig. S5. HRTEM images of selected regions with corresponding Fourier transform and lattice information.

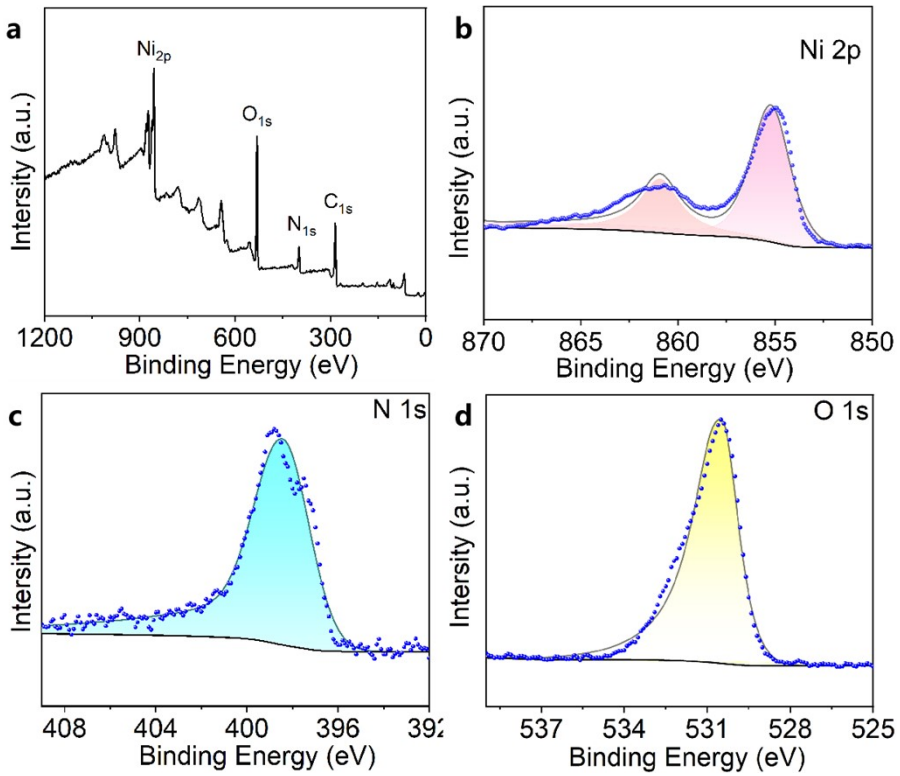

Fig. S6. (a) Full spectrum of XPS conducted on the samples, containing C, N, O and Ni elements. (b-d) High-resolution spectrums of Ni element, N element and O element, respectively.

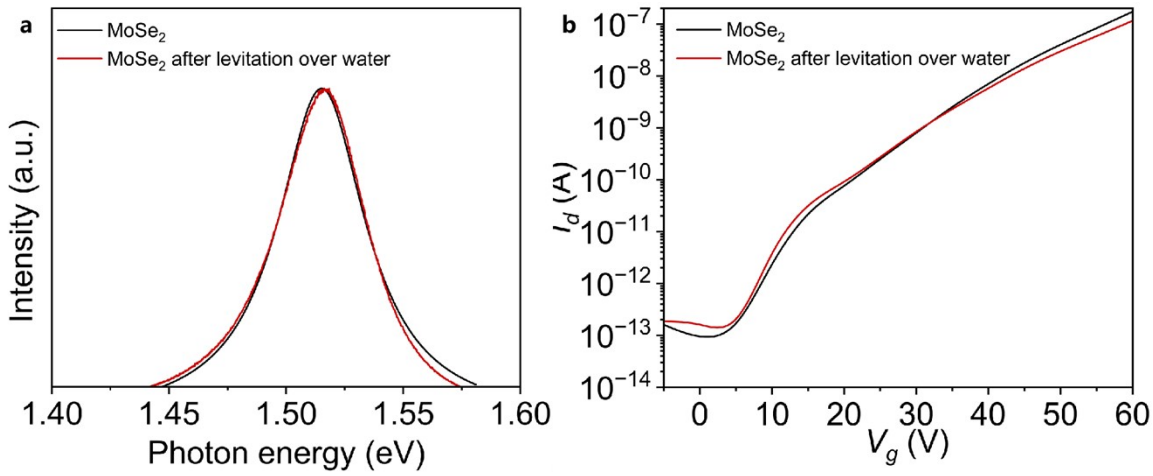

Fig. S7. Effect of water on material properties. (a) PL spectra and (b) Transfer characteristics of $MoSe_2$.

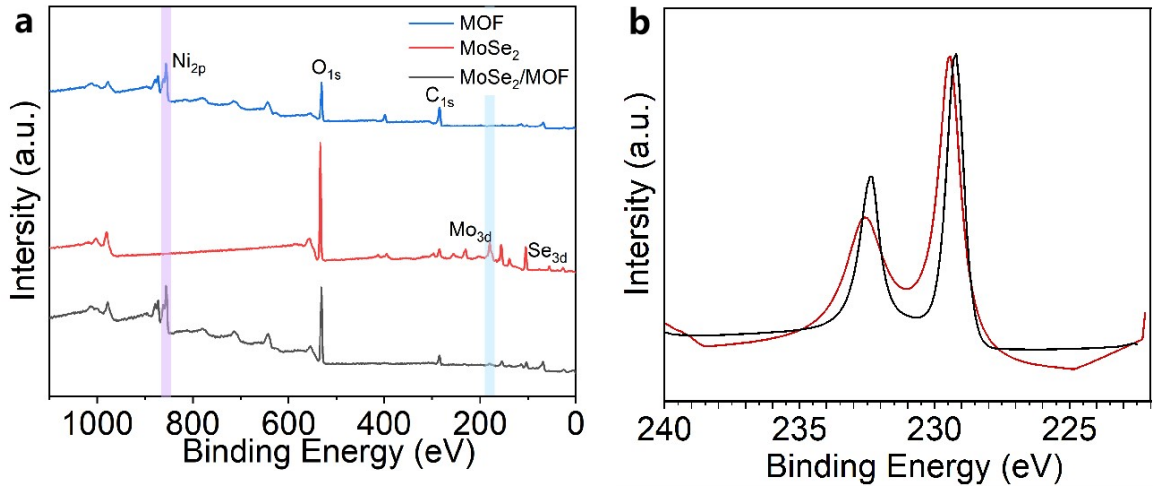

Fig. S8. (a) Comparison of XPS spectra of $MoSe_2$, Ni-MOF, and heterojunction. (d) Contribution of $Ni_3(HITP)_2$ on the XPS core-level spectra of Mo 3d of $MoSe_2$. Black and red are the heterostructures of $MoSe_2$, heterojunction, respectively.

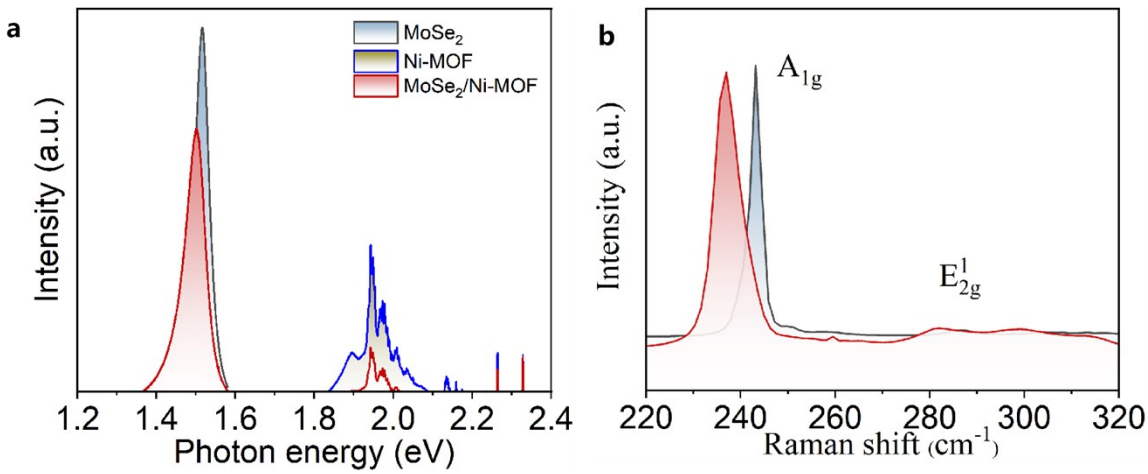

Fig. S9. (a) PL spectra and (b) Raman spectra of $MoSe_2$ and heterojunction measured.

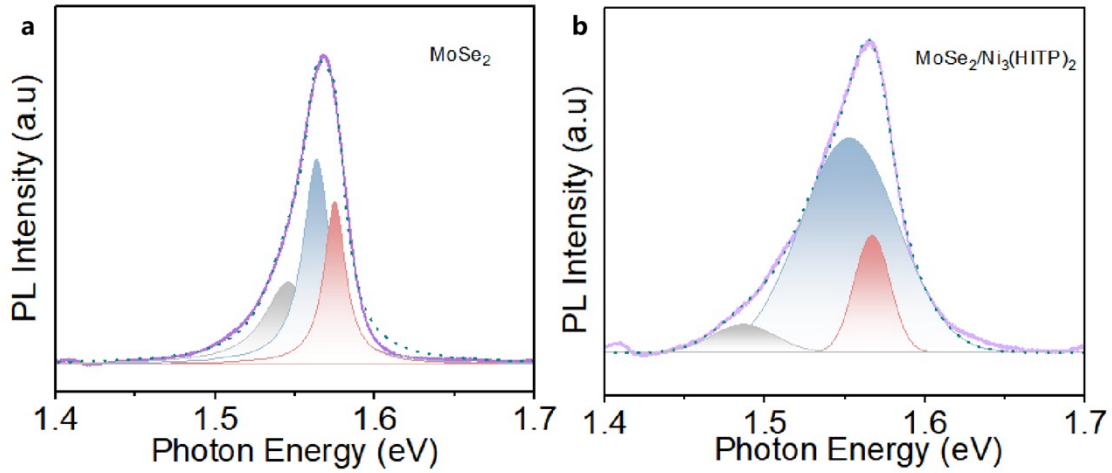

Fig. S10. PL spectra of (a) $MoSe_2$ and (b) heterojunction, fitted with a Lorentzian function to quantify the trion (X^-) weight.

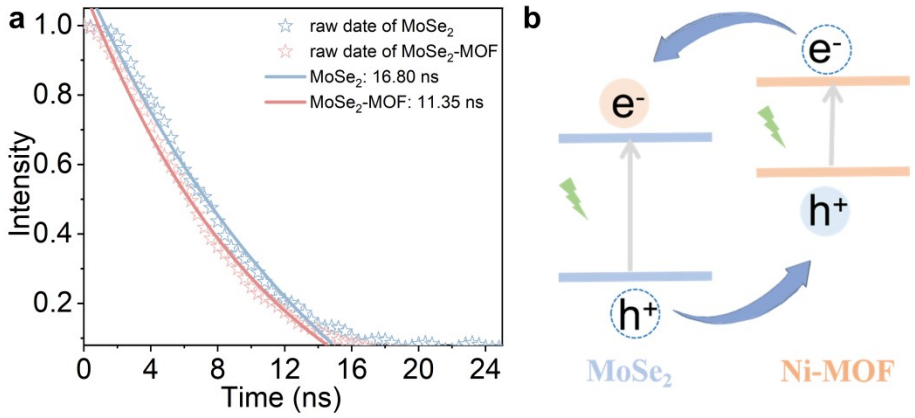

Fig. S11. (a) TRPL of $MoSe_2$ in monolayer and heterojunction. (b) Schematic of the charge transfer processes in heterostructures. The grey straight arrow represents the excitation.

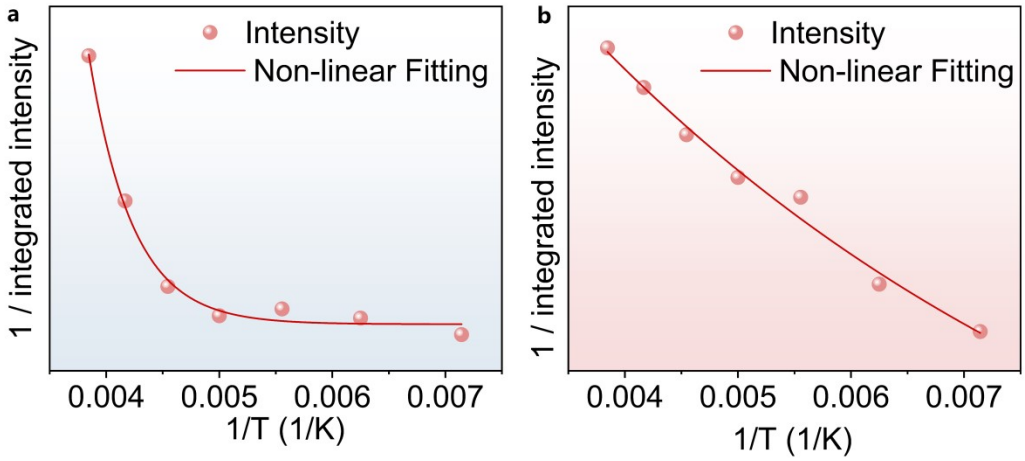

Fig. S12. Binding energy measurement. Integrated intensity to temperature plot of $MoSe_2$ and heterojunction. Based on nonlinear fitting, a E_B of 224.9 meV was obtained for $MoSe_2$. The E_B of the heterojunction was 26.2 meV.

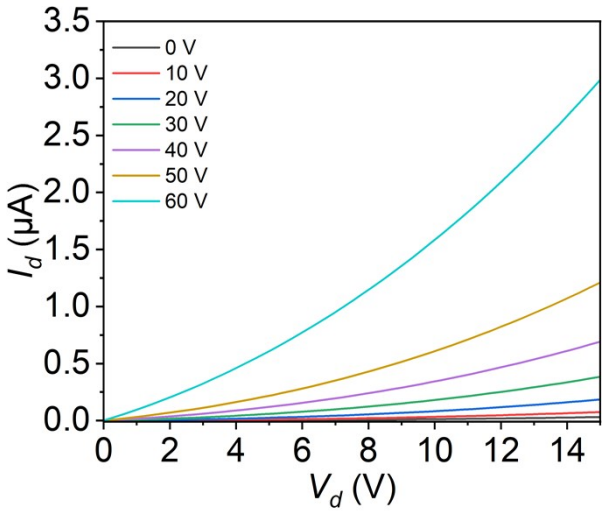

Fig. S13. The output curves of the heterojunction FET device. The device exhibits a favourable ohmic contact.

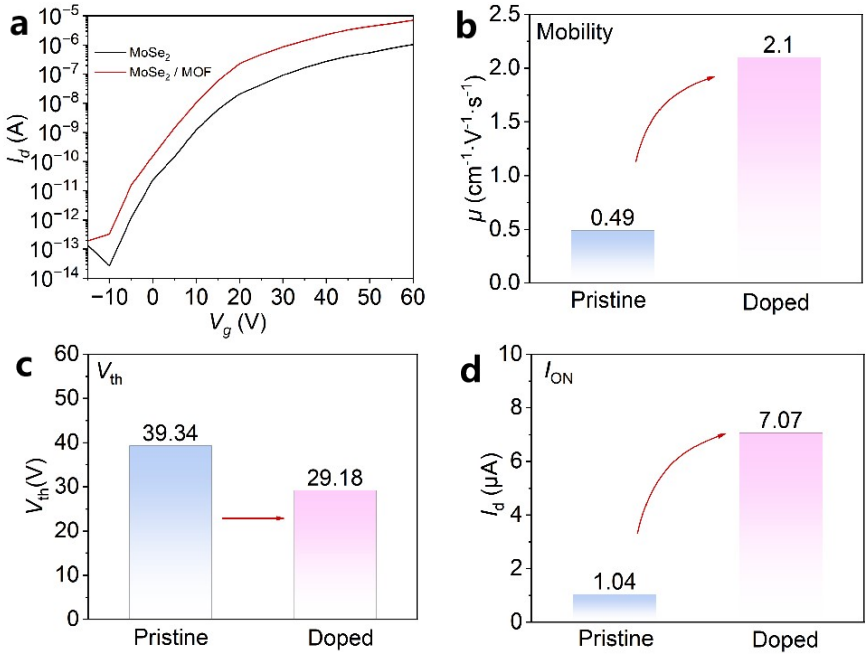

Fig. S14. (a)Transfer characteristics of $MoSe_2$ FET devices before (black line) and after (red line) *in situ* growing MOF. Visualisation of parameters (b) carrier mobility (c) threshold voltage and (d) current values different between $MoSe_2$ and heterojunction.

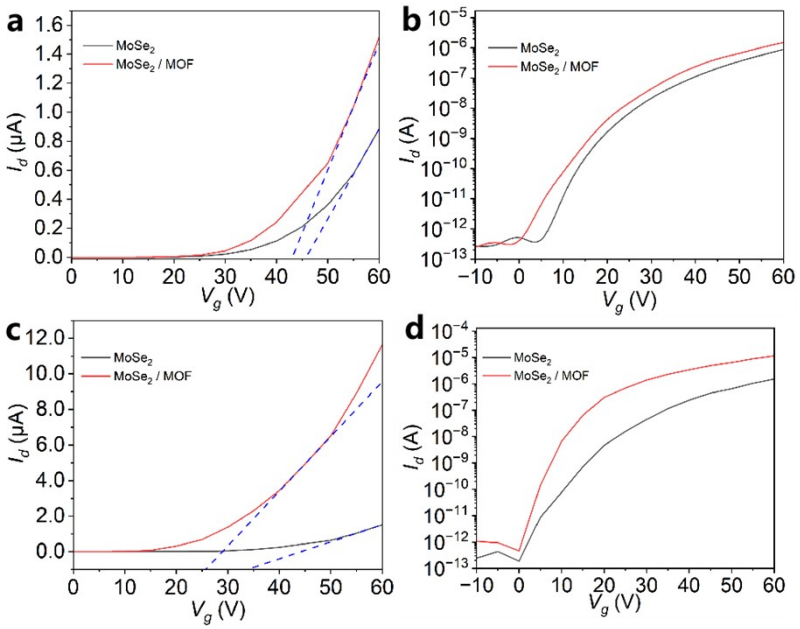

Fig. S15. Transfer characteristics of different $MoSe_2$ FET devices before (black line) and after (red line) *in situ* growing MOF.

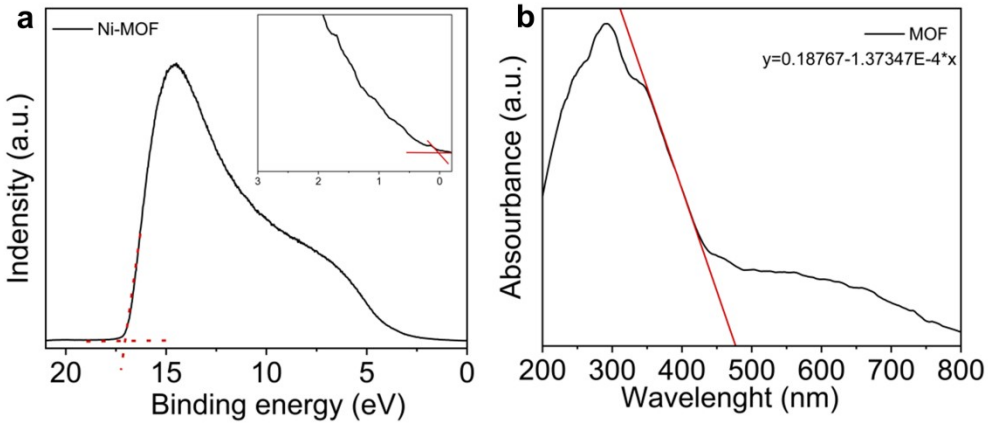

Fig. S16. Ultraviolet photoelectron spectroscopy and ultraviolet-visible spectroscopy of Ni-MOF.

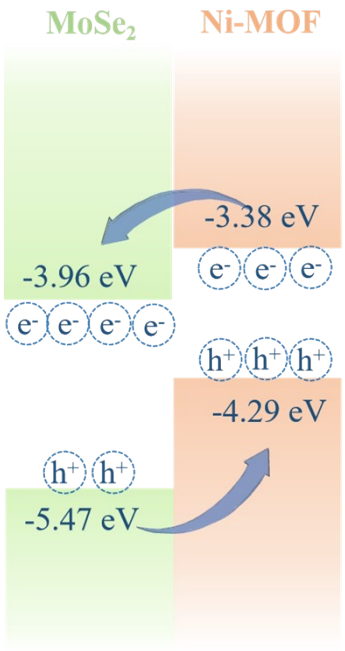

Fig. S17. Energy band alignment of $MoSe_2$ and Ni-MOF. The heterojunction formed by $MoSe_2$ and Ni-MOF is a type-II heterojunction.

The HOMO and LUMO energy level of the MOF film was calculated as:

$E_{eg}=h\nu=hc/\lambda=0.91$ eV; WF=21.22-17.03=4.19 eV; E_{HOMO} = -(4.19+0.1) eV=-4.29 eV; E_{LOMO} = -(4.29-0.91) eV=-3.38 eV

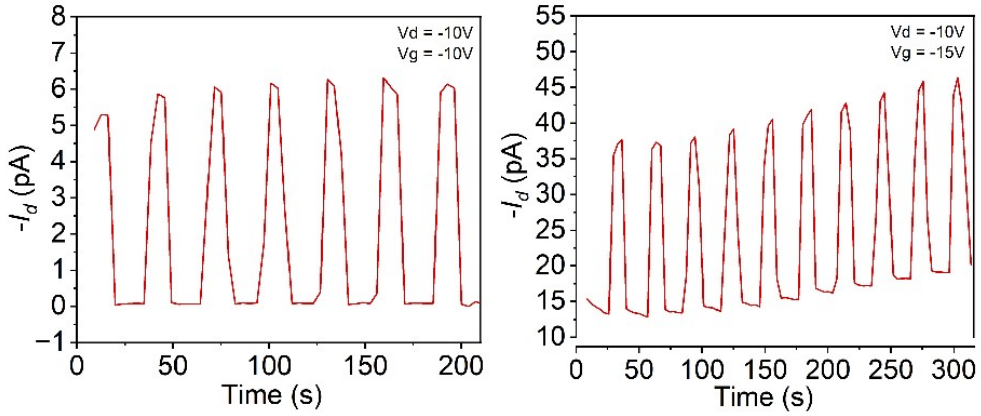

Fig. S18. Photoswitching response of heterojunctions.

Table S1. Comparison with Reported Mobility Enhancing Heterojunctions

material	V_d (V)	I_{on}/I_{off} increase	μ ($cm^2 V^{-1} s^{-1}$) increase	V_{th} (V) increase	ref
$MoSe_2$/Ni-MOF	10	579 %	328 %	10.16	This work
WSe_2/β-Ga_2O_3	1	247 %	39 %	0.4	1
WSe_2 UV/Ozone	2	~350 %	~400 %	33.5	2
MoS_2/2D TAPB-PDA	0.5	183 %	128 %	11	3
MoS_2/pentacene	50	N/A	25 %	14.79	4
4-NBD/WSe_2	-2	130 %	98 %	1.43	5

Table S2. Comparison of the Optical Response Ability of Existing Transistors

material	V_d (V)	wavelength (nm)	incident power (mW cm^{-2})	R (A W^{-1})	D* (Jones)	ref
$MoSe_2$/Ni-MOF	10	405	5	28.25	4.13×10^{11}	This work
$MoSe_2/Cu_2S$	-2	514	50	0.41	2.72×10^{12}	6
n-WS_2/p-PbS QDs	2	1550	N/A	0.18	4.11×10^{11}	7
$MoSe_2$	3	442	11.936	4.42	2.28×10^{11}	8
$MoSe_2$/GaAs	5	808	5.0×10^{-3}	5.25	1.13×10^{13}	9
MoO_3/MoS_2	-3	514	7.5	0.16	2.8×10^{11}	10

As shown in the comparison, our devices exhibit competitive performance. Therefore, this preparation strategy has the potential for developing optoelectronic devices.

1. S. Moon, J. Bae and J. Kim, *J. Mater. Chem. C*, 2022, **10**, 6281–6286.
2. S. Yang, G. Lee and J. Kim, *ACS Appl Mater Interfaces*, 2021, **13**, 955-961.
3. C. Wang, L. Cusin, C. Ma, E. Unsal, H. Wang, V. G. Consolaro, V. Montes-Garcia, B. Han, S. Vitale, A. Dianat, A. Croy, H. Zhang, R. Gutierrez, G. Cuniberti, Z. Liu, L. Chi, A. Ciesielski and P. Samori, *Adv Mater*, 2023, **36**, 2305882.
4. Q. Ren, Q. Xu, H. Xia, X. Luo, F. Zhao, L. Sun, Y. Li, W. Lv, L. Du, Y. Peng and Z. Zhao, *Organic Electronics*, 2017, **51**, 142-148.
5. S. Liu, X. Xiong, X. Wang, X. Shi, R. Huang and Y. Wu, *Sci China Inf Sci*, 2024, **67**, 160406:160402.
6. M. S. Hassan, S. Bera, D. Gupta, S. K. Ray and S. Sapra, *ACS Applied Materials & Interfaces*, 2019, **11**, 4074-4083.

7. S. H. Kim, D. Lee, S. Moon, J. H. Choi, D. Kim, J. Kim and S. W. Baek, *Advanced Functional Materials*, 2023, **33**, 2303778.
8. X. Zhao, X. Wang, R. Jia, Y. Lin, T. Guo, L. Wu, X. Hu, T. Zhao, D. Yan, L. Zhu, Z. Chen, X. Xu, X. Chen and X. Song, *RSC Advances*, 2024, **14**, 1962-1969.
9. S. Debnath, M. Meyyappan and P. K. Giri, *ACS Applied Materials & Interfaces*, 2024, **16**, 9039-9050.
10. S. Pal, S. Mukherjee, M. Nand, H. Srivastava, C. Mukherjee, S. N. Jha and S. K. Ray, *Applied Surface Science*, 2020, **502**, 144196.